pressure of 2 mtorr. The sputtering power and the deposition time was fixed as 100 W and 10 min, respectively.

Device Fabrication: The flexible OELD was prepared onto the PI substrate with the ITO film (anode) grown at 150 °C by an rf magnetron sputtering method. The OELD prepared in the present study consisted of a typical organic double-layer structure, having hole-transporting and electron-transporting/emitting layers between two electrodes: PI (250 μm)/ITO (120 nm)/HTL (40 nm)/ET&EML (70 nm)/Al (150 nm) device. *N*,*N*′-diphenyl-*N*,*N*′-(3-methylphenyl)-[1,1′-biphenyl]-4,4′-diamine (TPD) and tris(8-hydroxyquinolinato) aluminum (Alq_3) are used as HTL and ET/EML, respectively. The TPD, Alq_3, and aluminum (Al) cathode layers were prepared by a thermal evaporation method in a vacuum of ca. 10^{-6} torr, monitoring the film thickness in situ by a thickness monitor (STM-100/MF, Sycon Instruments Co.)

Measurements: The sheet resistance measurements were performed using a four-point probe. All sheet resistance values were determined as the average of three measurements for each film. The optical transmission spectra were measured with an UV-vis-near IR spectrophotometer (Varian, CARY 5E). The scan range and the rate of transmission measurement were 200–800 nm and 600 nm min^{-1}, respectively. X-ray diffraction (XRD) was used to characterize the crystal structure of the ITO films. The X-ray source used was Cu Kα radiation ($\lambda = 1.5406$ nm). From the analysis of the diffraction pattern, the preferred orientation and the average grain size of the ITO films were determined and calculated. The surface morphology of the ITO films were measured over a 2 × 2 μm^2 scan area by atomic force microscopy (AFM) (Nanoscope IIIa, Digital Instruments Co.). AFM was also used to estimate the thickness of the ITO, TPD, Alq_3, and Al layers, in which the tapping mode with a 125 μm long etched Si probe was used to avoid damage of the organic film surfaces during the scanning process. The current density–voltage–luminance (*J*–*V*–*L*) data was taken using an electrometer (Keithley 6517) and a photomultiplier tube (Hamamatsu Photonics Co.) along with a candela meter (BM-8, Topcon Instrument Co.). The electroluminescent (EL) spectrum of the device was measured by a high-sensitivity fiber optic spectrometer (S2000, Ocean Optics Inc.) with a 2048-element linear CCD-array silicon detector. Measurement of the *J*–*V*–*L* and the EL spectrum data was performed in a dark chamber under air at ambient conditions without charging inert gases.

Received: December 27, 2001
Final version: July 22, 2002

[1] I. Hamberg, C. G. Granqvist, *J. Appl. Phys.* **1986**, *60*, R123.
[2] H. L. Hartnagel, A. L. Dawar, A. K. Jain, C. Jagadish, *Semiconducting Transparent Thin Films*, Institute of Physics, Bristol, UK **1995**.
[3] Special Issue on Transparent Conducting Oxides (Eds: D. S. Ginley, C. Bright), *MRS Bull.* **2000**, *25(August)*.
[4] P. E. Burrows, G. Gu, V. Bulovic, Z. Shen, S. R. Forrest, M. E. Thompson, *IEEE Trans. Electron Devices* **1997**, *44*, 1188.
[5] C. W. Tang, S. A. VanSlyke, *Appl. Phys. Lett.* **1987**, *51*, 913.
[6] J. H. Burroughes, D. D. C. Bradley, A. R. Brown, R. N. Marks, K. Mackay, R. H. Friend, P. L. Burn, A. B. Holmes, *Nature* **1990**, *347*, 539.
[7] D. Braun, A. J. Heeger, *Appl. Phys. Lett.* **1991**, *58*, 1982.
[8] G. Grem, G. Leditzky, B. Ullrich, G. Leising. *Adv. Mater.* **1992**, *4*, 32.
[9] G. Gustaffson, Y. Cao, G. M. Treacy, F. Klavertter, N. Colarneri, A. J. Heeger, *Nature* **1992**, *357*, 477.
[10] P. May, *SID Int. Symp., Dig. Tech. Papers* **1996**, *27*, 192.
[11] S. Yamamoto, T. Yamanaka, Z. Ueda, *J. Vac. Sci. Technol.* **1987**, *A5*, 1957.
[12] T. Minami, H. Sonohara, T. Kakumu, S. Takata, *Thin Solid Films* **1995**, *270*, 37.
[13] B. D. Cullity, S. R. Stock, *Elements of X-ray Diffraction*, Prentice Hall, Englewood Cliffs, NJ **2001**.
[14] W. F. Wu, B. S. Chiou, *Thin Solid Films* **1997**, *298*, 221.
[15] Z. W. Yang, S. H. Han, T. L. Yang, L. Ye, D. H. Zhang, H. L. Ma, C. F. Cheng, *Appl. Surf. Sci.* **2000**, *161*, 279.
[16] D. Wilson, H. Stenzenberger, P. Hergenrother, *Polyimides*, Blackie and Son, London **1990**.
[17] R. A. Dine-Hart, W. W. Wright, *Makromol. Chem.* **1971**, *143*, 189.
[18] S. Itamura, M. Yamada, S. Tamura, T. Matsumoto, T. Kurosaki, *Macromolecules* **1993**, *26*, 3490.
[19] T. Matsumoto, T. Kurosaki, *Macromolecules* **1997**, *30*, 993.
[20] T. Matsuura, Y. Hasuda, S. Nishi, N. Yamada, *Macromolecules* **1991**, *24*, 5001.
[21] G. Hougham, G. Tesoro, J. Shaw, *Macromolecules* **1994**, *27*, 3642.
[22] J. Kato, A. Seo, S. Shiraishi, *Macromolecules* **1999**, *32*, 6400.
[23] T. Matsuura, S. Ando, S. Matsui, S. Sasaki, F. Yamanoto, *Electron. Lett.* **1993**, *29*, 2107.
[24] S. Ando, T. Sawada, Y. Inoue, *Electron. Lett.* **1993**, *29*, 2143.
[25] S. Matsuda, S. Ando, T. Sawada, *Electron. Lett.* **2001**, *37*, 706.
[26] A. F. Mayadas, M. Shatzkes, *Phys. Rev.* **1970**, *B1*, 1382.
[27] A. K. Kulkarni, K. H. Schulz, T. S. Lim, M. Khan, *Thin Solid Films* **1999**, *345*, 273.
[28] H. Kim, C. M. Gilmore, A. Pique, J. S. Horwitz, H. Mattoussi, H. Murata, Z. H. Kafafi, D. B. Chrisey, *J. Appl. Phys.* **1999**, *86*, 6451.
[29] D. B. Fraser, H. D. Cook, *J. Electrochem. Soc.* **1972**, *119*, 1368.
[30] G. Haacke, *J. Appl. Phys.* **1976**, *47*, 4086.
[31] W. F. Wu, B. S. Chiou, S. T. Hsieh, *Semicond. Sci. Technol.* **1994**, *9*, 1242.
[32] C. W. Tang, *SID Int. Symp. Dig. Tech. Papers* **1996**, 27, 181.
[33] S. Miyata, H. S. Nalwa, *Organic Electroluminescent Materials and Devices*, Gordon and Breach, Singapore **1997**.

Directed Colloidal Assembly of 3D Periodic Structures**

By *James E. Smay*, *Gregory M. Gratson*, *Robert F. Shepherd*, *Joseph Cesarano III*, and *Jennifer A. Lewis**

Three-dimensional periodic structures fabricated from colloidal "building blocks" may find widespread technological application as advanced ceramics,[1] sensors,[2] composites,[3] tissue engineering scaffolds,[4] and photonic[5] materials. Several strategies have recently been developed for precisely positioning colloidal particles in both two-[6] and three-dimensional[7] (2D/3D) arrays. These approaches commonly rely on first creating patterned substrates via photolithography[6g,7a] or microcontact printing (μCP).[6a–f,7b] Such surfaces direct colloidal assembly either epitaxially, i.e., as particles pack into cavities, or through electrostatic interactions between oppositely charged particles and patterned features (e.g., self-assembled monolayers or polyelectrolyte species) on the substrate surface. Of these, only colloidal epitaxy has been used to guide the assembly of 3D periodic structures, which consist of colloidal crystals with a lattice constant on the order of the colloidal dimensions.[7] Many targeted applications,[1–4] however, require periodicity at length scales far exceeding colloidal dimensions with lattice constant(s) ranging from several micrometers to millimeters.

Direct-write techniques,[8–10] such as robocasting,[9] ink jet printing,[10a] hot-melt printing,[10b] and micropen writing[10c] involve assembly via a layer-by-layer deposition of colloidal-based inks. Such techniques offer a powerful alternative for

[*] Prof. J. A. Lewis, J. E. Smay,[+] G. M. Gratson, R. F. Shepherd
Department of Materials Science and Engineering
University of Illinois at Urbana-Champaign
1304 West Green Street, Urbana, IL 61801 (USA)
E-mail: jalewis@staff.uiuc.edu
Dr. J. Cesarano III
Sandia National Laboratories
1001 University Blvd., SE, Albuquerque, NM 87106 (USA)
[+] Present address: School of Chemical Engineering, Oklahoma State University, Stillwater, OK 74078, USA.

[**] This work was funded by the National Science Foundation (Grant# DMI 00-99 360). J. A. Lewis acknowledges partial support from the U.S. Department of Energy, Division of Materials Sciences through the Frederick Seitz MRL at UIUC. G. M. Gratson thanks the U. S. Department of Defense for an NDSEB research fellowship. We thank Profs. C. Zukoski, P. Wiltzius, and K. Suslick for valuable discussions.

  0935-9648/02/1809-1279 $ 17.50+.50/0

ADVANCED MATERIALS

producing complex 3D structures, including space-filling solids and structures with high aspect ratio walls or spanning (unsupported) elements. The latter structure, which exhibits the desired 3D periodicity, places the most stringent demands on ink design. Several ink designs have been explored including dispersed colloidal fluids,[10a] highly shear thinning colloidal suspensions,[9,10c] and colloid-filled organic inks.[10b] Such inks solidify either by liquid evaporation[9,10a,c] or a temperature-induced phase change.[10b] For example, robocasting[9a,b] involves the deposition of highly concentrated inks that undergo a drying-induced pseudoplastic to dilatent transition. These inks are well suited for assembly of space-filling solids.[9c] However, they are incapable of fully supporting their own weight during assembly of spanning structures due to their initial fluidity and difficulties associated with controlling drying kinetics during multilayer fabrication.

Here, we develop concentrated colloidal inks with interparticle interactions tailored specifically for robotic deposition (Scheme 1) of 3D periodic structures with self-supporting features. These inks must satisfy two important criteria. First, they must exhibit a well-controlled viscoelastic response, i.e., they flow through the deposition nozzle and then "set" immediately to facilitate shape retention of the deposited features even as it spans gaps in the underlying layer(s). Second, they must contain a high colloid volume fraction to minimize drying-induced shrinkage after assembly is complete, i.e., the particle network is able to resist compressive stresses arising from capillary tension.[11] These criteria require careful control of colloidal forces to first generate a highly concentrated, stable dispersion followed by inducing a system change (e.g., ΔpH, ionic strength, or solvent quality) that promotes the fluid-to-gel transition illustrated schematically in Figure 1a.

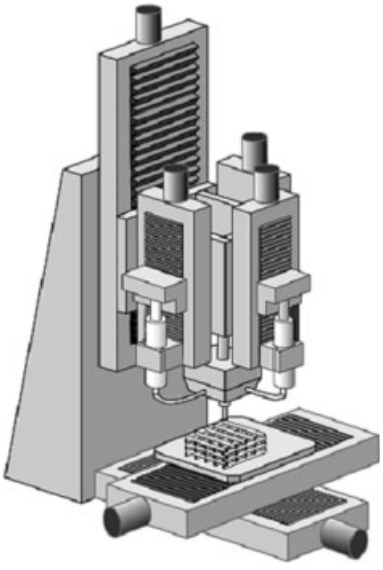

Scheme 1. Schematic illustration of the robotic deposition apparatus used in the directed assembly of concentrated colloidal gel-based inks. Inks are housed in individual syringes mounted on the *z*-axis motion stage, and deposited through a cylindrical nozzle (diameter ranging from 100 μm to 1 mm) onto a moving *x*–*y* stage. Typical build times for the mesoscale periodic structures illustrated in subsequent figures are ~10 min/part at an *x*–*y* table speed of 5 mm s^{-1}. (Note: Structures were assembled in a low viscosity oil reservior (not shown) placed on the *x*–*y* stage.)

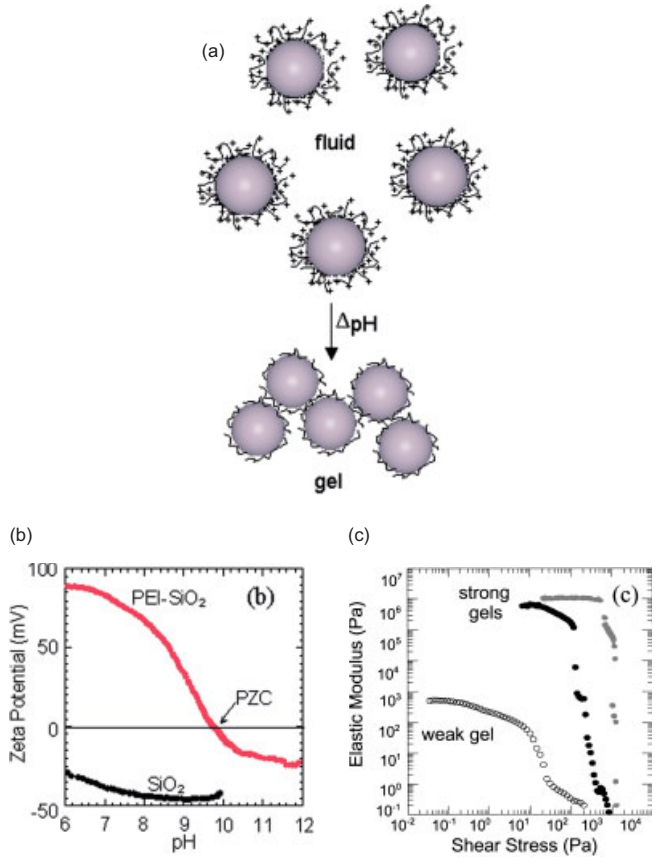

Fig. 1. a) Schematic illustration of the fluid-to-gel transition observed for colloidal inks. b) A plot of zeta potential versus pH for bare and PEI-coated silica microspheres suspended in water. c) The corresponding log–log plot of their shear elastic modulus versus shear stress for concentrated silica gels of varying strength: open symbols denote weak gel (pH 9.50), black symbols denote strong gel (pH 9.75), and gray symbols denote strong gel (in oil). (Note: The point-of-zero charge for PEI-coated silica microspheres occurs at pH 9.75, which is significantly above the value (~pH 2–3) observed for bare silica particles. The weak gel had insufficient strength to support its own weight during deposition. The mechanical properties of the strong gel were enhanced when the aqueous fluid was replaced by oil.)

We demonstrate this ink design using a model system comprised of polyethyleneimine (PEI)-coated silica microspheres, whose interactions were carefully modulated by changing solution pH. PEI is a highly branched polyamine that contains primary, secondary, and tertiary amine groups in a ~1:2:1 ratio. Over the pH range of interest, PEI is positively charged with approximately 50 % of these groups protonated at ~pH 6.[12] Bare silica microspheres are highly negatively charged over this pH range, as shown in Figure 1b. Due to strong electrostatic interactions between these oppositely charged species, PEI adsorbs strongly onto the silica microspheres inducing charge reversal at pH 7 followed by subsequent charge neutralization at ~pH 10, as the number of protonated groups along the PEI backbone decreases.[12] This latter pH coincides with the point-of-zero charge (PZC) for the PEI-coated silica microspheres, as shown in Figure 1b. In

  0935-9648/02/1809-1280 $ 17.50+.50/0 *Adv. Mater.* **2002**, *14*, No. 18, September 16

the absence of electrostatic repulsion, colloidal interactions are dominated by long-range van der Waals forces driving the microspheres into a highly flocculated state under these conditions. This mechanism for tuning interparticle forces can be readily extended to colloidal particles with alternate surface chemistry (i.e., basic surfaces) through the selection of an appropriately charged, anionic polyelectrolyte, such as poly(acrylic acid).

In our approach, we first generated a well dispersed silica suspension (pH 7) to facilitate the high solids loading (> 45 %) required, followed by inducing a fluid-to-gel transition (~pH 10) to generate the desired viscoelastic response. A dramatic rise in elastic properties accompanied this phase transition, as shown in Figure 1c. Both the shear yield stress and elastic modulus increased by orders of magnitude due to strengthened interparticle attractions near this pH value,[1a] as given by the following scaling relationship:[13]

$$y = k\left(\frac{\phi}{\phi_{gel}} - 1\right)^{x} \quad (1)$$

where y is the elastic property of interest (shear yield stress (τ_y) or elastic modulus (G'), k is a constant, ϕ_{gel} is the colloid volume fraction at the gel point, and x is the scaling exponent (~2.5). The equilibrium mechanical properties of colloidal gels are governed by two parameters: ϕ, which is proportional to their bond density, and ϕ_{gel}, which scales inversely with bond strength. Because interparticle attractions intensify as pH approaches the PZC, colloidal gels (of constant ϕ) experienced significant increases in their elastic properties.

Concentrated silica gels (pH 9.75) were utilized as inks for directed assembly of the 3D periodic structures shown in Figures 2 and 3. The ink was robotically deposited onto a moving x–y stage yielding a 2D pattern (Scheme 1). After a given layer was generated, the stage was incremented in the z-direction (Δz) and another layer was deposited. This process was repeated until the desired 3D structure was created. The ink flowed through the nozzle at the volumetric flow rate required to maintain a constant deposition speed (v) of 5 mm s^{-1}. As the ink exits the nozzle, it forms a continuous, rod-like filament with a rigid (gel) core–fluid shell architecture that simultaneously promotes shape retention while allowing the rods to fuse together at their contact points. This filamentary architecture arises because the percolating network of attractive particles within the gelled ink is capable of transmitting stress above ϕ_{gel}. When stressed beyond its yield point (τ_y), the ink exhibits shear thinning flow behavior due to the attrition of particle–particle bonds within the gel, as described by:[14]

$$\tau = \tau_y + K\dot{\gamma}^{n} \quad (2)$$

where τ is the shear stress, n is the shear thinning exponent (<1), K is the viscosity parameter, and $\dot{\gamma}$ is the shear rate. This behavior is reflected in the rheological response shown in Figure 1c. Below τ_y, G' is independent of applied stress (i.e., the system resides in the linear viscoelastic region). Above τ_y, interparticle bonds rupture leading to a sharp decrease in G' is needed to facilitate flow. To maintain constant ink composition (ϕ) and, thus, prevent changes in ink rheology due to water evaporation during assembly, the deposition process was carried out in an oil reservoir. The 3D structures were removed from this reservoir after assembly was completed and then dried under ambient conditions.

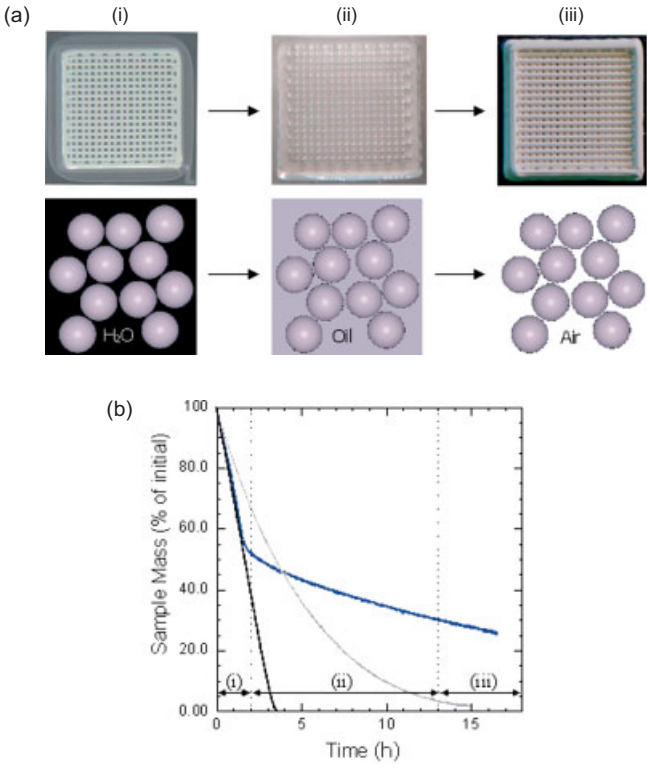

Fig 2. a) Optical images of a 3D periodic lattice assembled from concentrated colloidal silica gels (pH 9.75), which experienced a transition from an initially opaque state (i) to a translucent state (ii) to a final opaque state (iii), and their corresponding compositional evolution (illustrated schematically) arising from invasion percolation phenomena experienced during the drying process. b) Weight loss behavior of the 3D structure during drying (blue curve) plotted alongside the weight loss observed for both pure water (black curve) and the lower volatility oil (gray curve). The optical transitions described in part (a) are highlighted.

Optical images and weight loss data of representative 3D structures were acquired continuously during drying. Such structures experienced dramatic changes in their optical properties as drying proceeded (Fig. 2a). These observations indicate that water evaporation is first accompanied by oil invasion[15] into the pore network between colloidal particles. This phenomena gives rise to a translucent 3D structure at intermediate drying times (denoted by (ii) in Fig. 2b) due to refractive index matching between the silica microspheres and oil. Weight loss data (Fig. 2b) illustrates the accompanying transition from a constant rate period of drying (water evaporation) to a falling rate period of drying (due primarily to oil evaporation) that is nearly coincident with the observed transition in optical properties. Ultimately, the 3D structure returns to an opaque state, as oil evaporates creating an empty (air-filled) pore network at the culmination of the drying process.

  0935-9648/02/1809-1281 $ 17.50+.50/0

ADVANCED MATERIALS

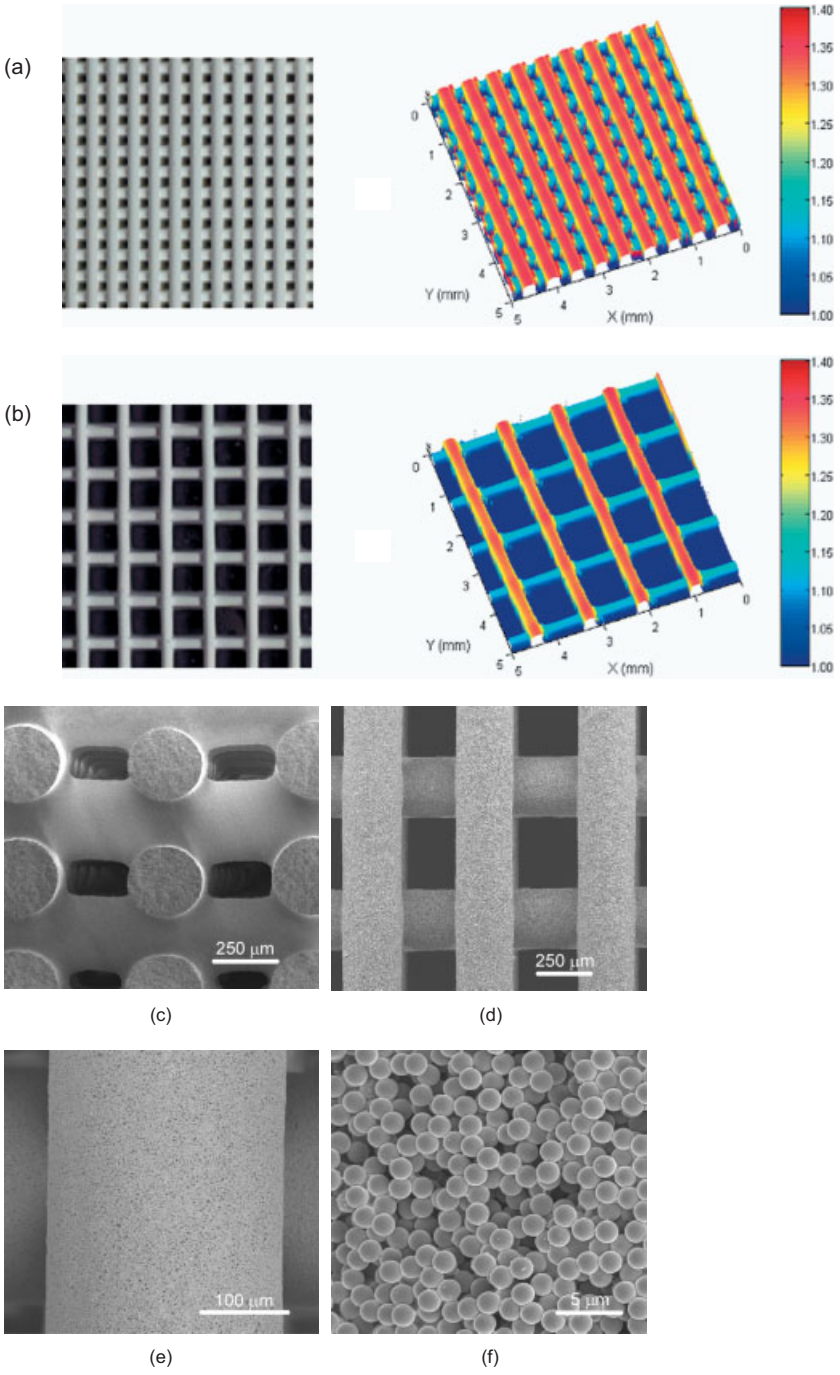

Fig. 3. Optical micrographs of 3D periodic lattices assembled from concentrated colloidal silica gels (pH 9.75) and corresponding profilometry scans of their top surfaces for a) simple cubic geometry with $D = 250$ μm, $d = 500$ μm, and # of layers = 10 and b) simple tetragonal layer (#10) and underlying (layer #9) layers is indicated by the accompanying color bars. c–f) Scanning electron micrographs of a simple cubic lattice structure (a) acquired at different magnifications. The deposited rods maintain their cylindrical shape upon deposition and drying, as shown in the cross-sectional image (c). The highest magnification image (f) illustrates the colloidal gel network that persists upon drying.

3D periodic structures were fabricated with varying center-to-center distance between rods to illustrate the ability of strong silica gels to span unsupported regions (Fig. 3). A comparison of the optical images and corresponding laser profilometry scans (Fig. 3a,b) of fully dry structures reveals that rods deposited on the top and underlying layers exhibited excellent height uniformity even across spanning distances approaching 1 mm. Higher magnification views of the simple cubic lattice (Fig. 3c–f) illustrate their cylindrical rod-like features, which are preserved during the assembly and drying processes, their smooth exterior surfaces, and the disordered particle network that comprises each spanning element.

The deflection of the spanning rods can be estimated in the small strain limit by applying a simply supported beam with a distributed load model, as given by:[16]

$$z_{\max} = \frac{-5Wd^4}{384EI} \tag{3}$$

where z_{max} is the maximum rod deflection in a given layer, W is the distributed load ($0.25\ \pi\rho_{\text{eff}}gD^2$), ρ_{eff} is the effective ink density ($=\rho_{\text{ink}}-\rho_{\text{oil}}$), g is the gravitational constant, D is the rod diameter, d is the span distance between rods, E is the Young's modulus ($=2G'(1+\nu)$) and I is the moment of inertia of the circular cross section ($=\pi D^4/64$). A more detailed analysis is provided by Smay et al.[17] A maximum spanning distance of ~5 mm was calculated for silica gels assembled in oil with G' of 0.5 MPa and a Poisson's ratio (ν) of ~0.5 using a criteria of $z_{\max} \leq -0.05D$, where $D = 250$ μm, $\rho_{\text{ink}} = 1.625\ \text{g cm}^{-3}$ and $\rho_{\text{oil}} = 0.762\ \text{g cm}^{-3}$. A solid filling fraction as low as 4 % can be achieved under these conditions. It should be noted that transient compositional changes arising during drying do not deleteriously affect their spanning ability (Fig. 1c).

This directed assembly approach is robust due to the generality of our ink design. Inks can be produced from any colloidal material provided their interparticle forces can be tuned to yield the desired viscoelastic response. The minimum ink elasticity required to assemble a given periodic structure can be estimated by setting $z_{\max} = -0.05D$, $s = d/D$, and rearranging Equation 3 as follows:

$$G' < 1.4\rho_{\text{eff}}\, gs^4 D \tag{4}$$

where s is the normalized span distance ($s < 1$ for spanning structures). Stronger inks must be formulated as the effective ink density, rod diameter, and normalized span distance increases. These parameters are independent of colloid size, polydispersity, and morphology, therefore, colloidal inks can be created from a broad array of particulate materials (e.g., ceramic, metallic, and polymeric colloids). With

  0935-9648/02/1809-1282 $ 17.50+.50/0 *Adv. Mater.* **2002**, *14*, No. 18, September 16

this as a guideline, we have developed suitable inks from a broad array of materials, including those based on ferroelectric,[17] structural, and biocompatible ceramics, where the colloidal particles were neither monodisperse nor spherical.

In summary, we have demonstrated a new route for assembling 3D periodic structures that involves direct patterning of colloidal inks within a non-wetting fluid reservoir. Concentrated colloidal gels with the appropriate viscoelastic behavior were robotically deposited to form spanning structures with characteristic feature sizes ranging from ~100 μm to 1 mm. This approach opens up an unexplored route for engineering complex 3D structures from colloidal building blocks.

Experimental

Concentrated silica dispersions were prepared by first adding an appropriate amount (0.5 mg m^{-2} silica) of polyethylenimine (PEI, $M_w = 2000$ g/mol; Aldrich Chemical Co., Milwaukee, WI) to deionized water at pH 7. PEI, which is a moderately charged cationic polyelectrolyte, served as the adsorbing layer. All pH adjustments were made using certified 1.0 N KOH and HNO_3 (Fisher Scientific). An appropriate amount of monodisperse silica microspheres ($D = 1.17 \pm 0.02$ μm, $\rho = 2.25$ g cm^{-3}, and specific surface area of 2.67 $m^2 g^{-1}$; GelTECH, Orlando, FL) was then added to the solution. The suspension was sonicated (Model 550 Sonic Dismembrator; Fisher Scientific, Pittsburgh, PA) for 10 min with a 1 s on/off pulse sequence at 20 kHz. The pH was then readjusted to 7, and the suspension was allowed to stir for 16 h on a magnetic stir plate. This procedure created a uniform dispersion of silica microspheres in suspension. The suspension was then sonicated once more followed by a final pH adjustment to ~10 to induce the desired fluid-to-gel transition. The resulting colloidal gel was homogenized, an aliquot of cellulose (Methocel F4 M; Dow Chemical Co., Midland, MI) stock solution was added to yield a final cellulose concentration of 5 mg mL^{-1}, and the gel was once again homogenized by high-shear agitation. Cellulose acted as a thickening agent, which increased the solution viscosity from ~1 mPa s to 30 mPa s to reduce the flocculation kinetics. This allowed the rigid core–fluid shell architecture of the deposited filaments to persist thereby promoting rod–rod adhesion.

Zeta potential (ξ) measurements (ESA 9800; Matec Applied Science, Northboro, MA) were carried out on a pure silica and silica–PEI suspensions ($\phi = 0.01$) as a function of pH.

Concentrated silica gels ($\phi = 0.46$) were prepared for rheological characterization and robotic deposition following the procedure outlined, which yielded gels of varying strength: 1) weak gel (pH 9.50) and 2) strong gel (pH 9.75). In addition, an oil-based, concentrated silica gel ($\phi = 0.46$) was also prepared for rheological characterization via controlled invasion of an appropriate volume of the strong gel (pH 9.75) with the oil phase. The shear elastic modulus (G') and yield stress (τ_y) were measured using a controlled stress rheometer (Bohlin CVOR-200, Cranbury, NJ) fitted with a concentric cylinder geometry (C-14). The C-14 bob was roughened with periodic grooves to mitigate possible wall-slip effects [18]. Oscillatory measurements were carried out at 1 Hz and a stress sweep was performed in ascending order. Prior to each measurement, a pre-shear of 200 s^{-1} was applied for 300 s followed by a 7200 s equilibration time to ensure a uniform shear history and that the suspension had reached equilibrium. All measurements were carried out at a constant temperature of 22 °C.

Mesoscale periodic lattices were assembled using a robotic deposition apparatus (JL2000, Robocasting Enterprises, Inc., Albuquerque, NM). The 3-axis motion of the x–y and z-stages was independently controlled by a custom-designed, computer-aided program (RoboCAD 2.0) that allowed for the construction of complex, 3D architectures in a layerwise deposition scheme. The lattice structures produced consisted of a linear array of rods aligned with the x- or y-axis such that their orientation was orthogonal to the previous layer, with varying rod spacing (L) of 250 to 750 μm. The ink was housed in a syringe (barrel diameter = 4.6 mm, EFD Inc., East Providence, RI) and deposited through a tapered nozzle (diameter, $D = 250$ μm) at a volumetric flow rate ($= 0.25\pi D^2 v$) required to maintain a constant x–y table speed (v) of 5 mm s^{-1}. The deposition process was carried out under a non-wetting oil to prevent drying during assembly.

Optical images and weight loss during drying were captured simultaneously with a digital camera and analytical balance. Digital images were captured every 60 s and sample mass was captured every 10 s until weight loss ceased. The refractive indices of silica, water, and oil are 1.46, 1.37, and 1.49, respectively.

The height profiles of these 3D structures were measured using non-contact, laser profilometry (Model DRS-2000, CyberOptics Corp., Minneapolis, MN). This profilometer employs a digital triangulation sensor that works by projecting a 670 nm, 0.95 mW laser on the test specimen and calculating the distance from a reference point by determining where the diffuse reflected light falls on a pixelized-array detector. The laser spot diameter was nominally 30 μm throughout the working focal range of ±5 mm with ~10 μm distance resolution. A computer controlled x–y translation stage was used to raster the laser over a rectangular area (5×5 mm^2), capturing height information for each structure with a 10×10 μm^2 grid spacing.

SEM images were obtained with a Hitachi S-4700 Scanning Electron Microscope (Hitachi Ltd., Tokyo Japan). After fabrication and drying, structures were mounted and sputtered with gold for 1 min (Emitech K575 Sputter Coater, Emitech Ltd., Ashford Kent, UK) prior to imaging.

Received: March 20, 2002
Final version: July 2, 2002

[1] a) J. A. Lewis, *J. Am. Ceram. Soc.* **2000**, *83*, 2341. b) V. Tohver, J. E. Smay, A. Braem, P. V. Braun, J. A. Lewis, *Proc. Natl. Acad. Sci.* **2001**, *98*, 8950.
[2] a) J. F. Tressler, S. Alkoy, A. Dogan, R. E. Newnham, *Composites: Part A* **1999**, *30*, 477. b) M. Allahverdi, S. C. Danforth, M. Jafari, A. Safari, *J. Eur. Ceram. Soc.* **2001**, *21*, 1485.
[3] a) M. P. Rao, A. J. Sanchez-Herencia, G. E. Beltz, R. M. McMeeking, F. F. Lange, *Science* **1999**, *286*, 102. b) R. Soundararajan, G. Kuhn, R. Atisivan, S. Bose, A. Bandyopadhyay, *J. Am. Ceram. Soc.* **2001**, *84*, 509.
[4] T.-M. Chu, J. Halloran, S. J. Hollister, S. E. Feinburg, *J. Mater. Sci: Mater. in Med.* **2001**, *12*, 471.
[5] a) J. D. Joannopoulos, P. R. Villeneuve, S. Fan, *Nature* **1997**, *386*, 143. b) Y. A. Vlasov, X. Z. Bo, J. C. Sturm, D. J. Norris, *Nature* **2001**, *414*, 289.
[6] a) A. Kumar, H. A. Biebuyck, G. M. Whitesides, *Langmuir* **1994**, *10*, 1498. b) J. Tien, A. Terfort, G. M. Whitesides, *Langmuir* **1997**, *13*, 5349. c) J. Aizenberg, P. V. Braun, P. Wiltzius, *Phys. Rev. Lett.* **2000**, *84*, 2997. d) K. M. Chen, X. Jiang, L. C. Kimerling, P. T. Hammond, *Langmuir* **2000**, *16*, 7825. e) H. P. Zheng, I. Lee, M. F. Rubner, P. T. Hammond, *Adv. Mater.* **2002**, *14*, 569. f) I. Lee, H. P. Zheng, M. F. Rubner, P. T. Hammond, *Adv. Mater.* **2002**, *14*, 572. g) Y. Yin, Y. Xia, *Adv. Mater.* **2001**, *13*, 267.
[7] a) A. van Blaaderen, R. Ruel, P. Wiltzius, *Nature* **1997**, *385*, 321. b) K. H. Lin, J. C. Crocker, V. Prasad, A. Schofield, D. A. Weitz, T. C. Lubensky, A. G. Yodh, *Phys. Rev. Lett.* **2000**, *85*, 1770.
[8] D. B. Chrisey, *Science* **2000**, *289*, 879.
[9] a) J. Cesarano III, P. Calvert, *US Patent 6 027 326*, **2000**. b) J. Cesarano III, R. Segalman, P. Calvert, *Ceram. Ind.* **1998**, *148*, 94. c) B. A. Tuttle, J. E. Smay, J. Cesarano III, J. A. Voight, T. W. Scofield, W. R. Olsen, J. A. Lewis, *J. Am. Ceram. Soc.* **2001**, *84*, 872.
[10] a) J. H. Song, M. J. Edirisinghe, J. R. G. Evans, *J. Am. Ceram. Soc.* **1999**, *82*, 3374. b) K. A. M. Seerden, N. Reis, J. R. G. Evans, P. S. Grant, J. W. Halloran, B. Derby, *J. Am. Ceram. Soc.* **2001**, *84*, 2514. c) S. L. Morissette, J. A. Lewis, P. G. Clem, J. Cesarano III, D. B. Dimos, *J. Am. Ceram. Soc.* **2001**, *84*, 2462. d) E. Sachs, M. Cima, P. Williams, D. Brancazio, J. Cornie, *Trans ASME, J. Eng. Ind.* **1992**, *114*, 481. e) E. Sachs, M. Cima, P. Williams, D. Brancazio, J. Cornie, *Manufacturing Rev.* **1992**, *5*, 117.
[11] J. J. Guo, J. A. Lewis, *J. Am. Ceram. Soc.* **1999**, *82*, 2345.
[12] E. Poptoshev, P. M. Claesson, *Langmuir* **2002**, *18*, 2590.
[13] G. M. Channel, C. F. Zukoski, *AIChE J.* **1997**, *43*, 1700.
[14] W. H. Herschel, B. Bulkley, *Kolloid-Z.* **1926**, *39*, 291.
[15] a) D. Wilkinson, J. F. Willemsen, *J. Phys. A: Math. Gen.* **1983**, *16*, 3365. b) T. M. Shaw, *Phys. Rev. Lett.* **1987**, *59*, 1671.
[16] J. E. Shigley, C. R. Mischke, in *Mechanical Engineering Design*, McGraw Hill, New York **1989**, p. 738.
[17] J. E. Smay, J. Cesarano III, J. A. Lewis, *Langmuir* **2002**, *18*, 5429.
[18] R. Buscall, J. I. McGowan, A. J. Morton-Jones, *J. Rheol.* **1993**, *37*, 621.

  0935-9648/02/1809-1283 $ 17.50+.50/0